




The Generation Mechanism of Tracking Error During Acceleration or Deceleration Phase in Ultraprecision Motion Systems

Luyao Dai , Xin Li , Yu Zhu, *Member, IEEE*, Ming Zhang , and Chuxiong Hu , *Senior Member, IEEE*

Abstract—In this paper, the generation mechanism of the tracking error during the acceleration or deceleration phase in ultraprecision motion systems is studied. For the first time, the analytical relationship among the tracking error, a feedforward controller, a feedback controller, and a reference trajectory is presented. Quantitative analysis shows that the tracking error is approximately proportional to a specific derivative of trajectory with given feedback and feedforward controllers. Moreover, the tracking error in ultraprecision motion systems is also greatly influenced by the effect of zero-order hold and time delay, which necessitates jerk feedforward. The analysis not only explains the generation mechanism of the tracking error, but also provides a criterion to judge the accuracy of feedforward coefficients by the shape of a residual tracking error. Based on this criterion, a feedforward tuning algorithm using dichotomy is proposed. The simulation and experiment both well-validate the generation mechanism of the tracking error and the proposed feedforward tuning algorithm.

Index Terms—Feedforward tuning, generation mechanism, tracking error, ultraprecision motion systems.

I. INTRODUCTION

ULTRAPRECISION motion systems that can achieve nanoscale accuracy are used in state-of-the-art manufacturing equipment such as lithography tools [1]. To meet the stringent technical requirements including nanoscale accuracy, air bearings, or magnetic-levitated linear or planar motors are utilized, where friction from the environment is negligible. The operation circle of these motion systems usually consists of acceleration, constant velocity, and deceleration phase. A large tracking error during the acceleration or deceleration phase will lead to a large settling time, the time cost it takes

Manuscript received April 3, 2018; revised June 24, 2018 and September 19, 2018; accepted October 12, 2018. Date of publication October 31, 2018; date of current version April 30, 2019. This work was supported in part by the National Key Research and Development Program of China under Grant 2017YFB0310603-02. (Corresponding author: Xin Li.)

The authors are with the State Key Laboratory of Tribology and the Beijing Key Laboratory of Precision/Ultra-Precision Manufacture Equipment and Control, Department of Mechanical Engineering, Tsinghua University, Beijing 100084, China (e-mail: daily16@mails.tsinghua.edu.cn; lixin_09@mail.tsinghua.edu.cn; zhuyu@tsinghua.edu.cn; zm01@mails.tsinghua.edu.cn; cxhu@tsinghua.edu.cn).

Color versions of one or more of the figures in this paper are available online at <http://ieeexplore.ieee.org>.

Digital Object Identifier 10.1109/TIE.2018.2878114

for the tracking error to converge to an acceptable level after acceleration or deceleration, which enormously decreases throughput. Therefore, the attenuation of the tracking error during the acceleration or deceleration phase is of paramount importance.

Combined with feedback control, feedforward control is usually regarded as one of the most critical techniques to attenuate the tracking error during the acceleration or deceleration phase. In [2] and [3], a model-based feedforward control strategy is utilized and shows that snap (the fourth derivative of the reference trajectory) feedforward is required to further improve the tracking performance after the use of acceleration feedforward. Since the performance of acceleration and snap feedforward is still limited, in [4]–[7], a finite impulse response (FIR) filter is used in cooperation with acceleration and snap feedforward, which is constructed with difference operators of different orders and tuned by data-based methods. In [8], an adaptive feedforward strategy is proposed to tune an acceleration feedforward coefficient online with the recursive least squares algorithm. Iterative learning control (ILC) is also one of the most powerful feedforward control techniques used in ultraprecision motion control [9], [10], which utilizes the control signals in previous operation iterations to form the control signals in the current one. In practice, ILC is also often used in cooperation with model-based feedforward like acceleration and snap feedforward. In a sense, above-mentioned feedforward algorithms such as FIR, adaptive feedforward, and ILC can be regarded as approaches to compensate for imperfect model-based feedforward. However, these algorithms mainly focus on the attenuation of the tracking error that the generation mechanism behind it remains unknown.

In this paper, the analytical relationship among the tracking error, the feedforward controller, the feedback controller, and the reference trajectory is presented for the first time. Research shows that the tracking error is approximately proportional to a specific derivative of the reference trajectory with given feedback and feedforward controllers. Research also shows that due to the effect of zero-order hold (ZOH) and time delay, it is not snap but jerk feedforward that is required to further improve the tracking performance with a well-tuned acceleration feedforward. The analysis not only explains the generation mechanism of the tracking error, but also provides a criterion to judge the accuracy of feedforward coefficients by the shape of the residual tracking error. Based on this criterion, a feedforward tuning

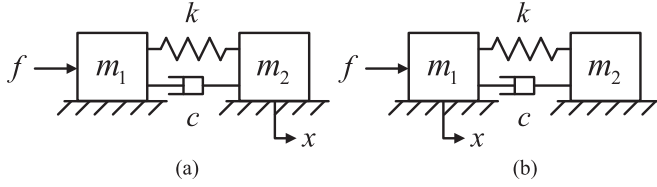


Fig. 1. Double-mass-block model. (a) Noncolocated system. (b) Colocated system.

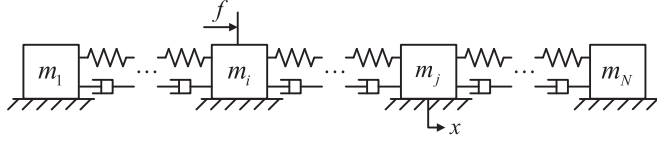


Fig. 2. Multimass-block model.

algorithm using dichotomy is proposed. The simulation and experiment both well validate the analysis on the generation mechanism and the proposed feedforward tuning algorithm.

II. GENERATION MECHANISM OF THE TRACKING ERROR DURING THE ACCELERATION OR DECELERATION PHASE

A. Plant Dynamics and Control Architecture

Ultraprecision motion systems, in practice, are usually actuated by levitated linear or planar motors, rendering friction from the environment negligible. Therefore, a double-mass-block model in Fig. 1(a) can be used to model the motion systems, which has one rigid body mode and one resonant mode. m_1 is the mass of the motor (mover of the motor indeed), m_2 is the mass of the load, k is the structural rigidity, c is the structural damping, f is the system input (force), and x is the system output (the displacement of load). The transfer function of the double-mass-block system is

$$G_p(s) = \frac{1}{(m_1 + m_2)} \frac{2\zeta_n \omega_n s + \omega_n^2}{s^2 (s^2 + 2\zeta_n \omega_n s + \omega_n^2)} = \frac{1}{(m_1 + m_2)} \left(\frac{1}{s^2} - \frac{1}{s^2 + 2\zeta_n \omega_n s + \omega_n^2} \right) \quad (1)$$

where ζ_n and ω_n are the damping ratio and the resonant frequency, respectively. The double-mass-block system is a widely used but simplified model; general friction-free ultraprecision systems can be modeled by the multimass-block system shown in Fig. 2, which consists of one rigid body mode and $N - 1$ resonant modes

$$G_p(s) = \frac{1}{ms^2} + \frac{1}{m} \sum_{i=1}^{N-1} \frac{\alpha_i}{s^2 + 2\zeta_i \omega_i s + \omega_i^2} \quad (2)$$

where m is the total mass of the whole system, N is the number of mass blocks, and ζ_i and ω_i are the damping ratio and the resonant frequency of the i th resonant mode, respectively. α_i is the model parameter determined by eigenmodes and positions of system input f and output x . Such systems can be further categorized into two classes: the noncolocated system and the colocated system. Fig. 1(a) and (b) shows noncolocated and colocated forms of the double-mass-block model, respectively.

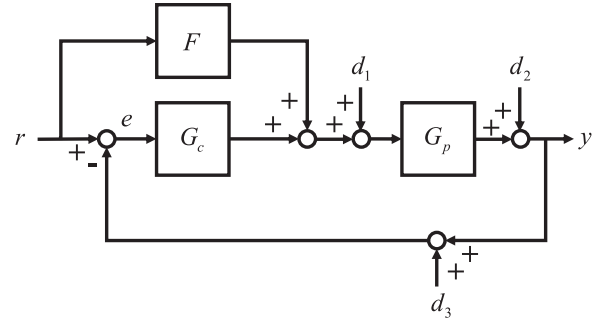


Fig. 3. Two-DOF control architecture.

TABLE I
MODEL PARAMETERS USED IN THE SIMULATION

m_1	m_2	k	c	ω_n	ζ_n
5 kg	20 kg	1.96×10^6 N/m	336 N · s/m	700 Hz	0.06

For friction-free motion systems, noncolocated and colocated systems share the same -40 -dB/dec rigid body dynamics at a low-frequency region, but differ at a higher frequency region. A detailed discussion on the dynamics of a general multimass-block model and colocated and noncolocated systems can be found in [11] and [12].

A two-degree-of-freedom (DOF) control strategy shown in Fig. 3 is a fundamental control architecture for such a kind of ultraprecision motion control. G_c is the feedback controller, F is the feedforward controller, G_p is the plant model, r is the reference trajectory, y is the system output, e is the tracking error, d_1 is the force disturbance, d_2 is the position disturbance, and d_3 is the sensor noise. The feedback controller is mainly utilized for system stabilization and disturbance rejection, while the feedforward controller for settling performance. The effect of disturbance and noise on the tracking error is out of consideration in this paper. Assuming that the plant model is invertible, the tracking error can be expressed as

$$e = \frac{G_p (G_p^{-1} - F)}{1 + G_p G_c} r = S_i (G_p^{-1} - F) r \quad (3)$$

where S_i is the input disturbance sensitivity function, which can be written as follows:

$$S_i = \frac{G_p}{1 + G_p G_c}. \quad (4)$$

Equation (3) explicitly shows that the tracking error is reduced to zero if $F = G_p^{-1}$, and thus, the design principle of the feedforward controller is to approximate the plant model inversion.

B. Simulation Parameters

Analysis in the next subsection is accompanied with a simulation. Simulation parameters are first given here before theoretical deductions. The model parameters used in the simulation are listed in Table I. The simulation is executed on the noncolocated form of the double-mass-block model shown in Fig. 1(a).

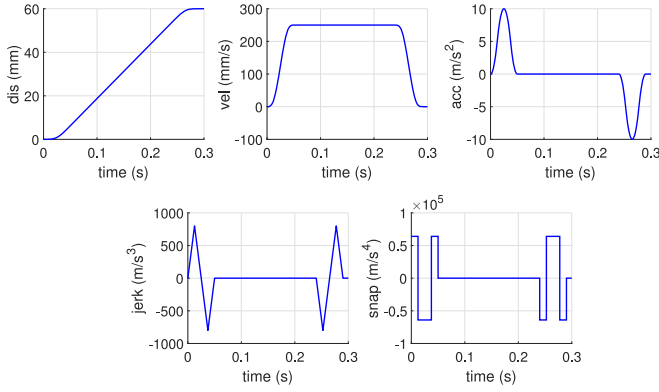


Fig. 4. Reference trajectory used in the simulation, dis bound 60 mm, vel bound 250 mm/s, acc bound 10 m/s², jerk bound 800 m/s³, and snap bound 64 000 m/s⁴.

A lead controller and a proportional–integral–differential (PID) controller are used as a feedback controller, standing for a feedback controller with a finite dc gain and an infinite dc gain, respectively. The transfer function of the lead controller is

$$G_c(s) = K \frac{s+z}{s+p}. \quad (5)$$

The transfer function of the PID controller is

$$G_c(s) = \left(k_p + \frac{k_i}{s} + k_d s \right) \frac{\omega_{lp}^2}{s^2 + 2\zeta_{lp}\omega_{lp}s + \omega_{lp}^2}. \quad (6)$$

A second-order low-pass filter is used in the PID controller to suppress high-frequency components of control signals. The control bandwidth (the crossover frequency at 0 dB in the bode diagram of an open-loop transfer function) in the simulation is 120 Hz. The fourth-order trajectory shown in Fig. 4(a) is used as the reference trajectory in the simulation. dis stands for displacement and derivatives from first to sixth orders are called vel, acc, jerk, snap, crackle, and pop. A detailed trajectory planning algorithm can be found in [13].

C. Quantitative Analysis of the Tracking Error

For simplicity and readability, here, analysis will mainly focus on the noncollocated form of the double-mass-block model shown in Fig. 1(a), but the results also apply for the general multimass-block model and the collocated system; general deductions will be given in Section II-F.

1) Approximation Formulas: The inversion of (1) can be expanded as a Taylor series at $s = 0$ as follows:

$$G_p^{-1}(s) = (m_1 + m_2) \left[s^2 + \frac{1}{\omega_n^2} s^4 - \frac{2\zeta_n}{\omega_n^3} s^5 + \dots \right]. \quad (7)$$

Since the reference trajectory mainly contains low-frequency components, low-order terms in the series expansion can give a good approximation of plant model inversion at a low-frequency region. Moreover, the input disturbance sensitivity function can be approximated by

$$S_i \approx \lim_{s \rightarrow 0} \frac{G_p(s)}{1 + G_p(s)G_c(s)} = \frac{1}{G_c(0)} \quad (8)$$

where $G_c(0)$ is the dc gain of the feedback controller. Note that if an integrator exists in the feedback controller, the dc gain will be infinite, and the approximation (8) no longer stands. If only one integrator exists, the approximation of the input disturbance sensitivity function should be revised as

$$S_i \approx \frac{s}{\tilde{G}_c(0)} \quad (9)$$

where $\tilde{G}_c(s) = sG_c(s)$.

The analysis on the tracking error is based on the above-mentioned approximation formulas. Since the approximation of the input disturbance sensitivity function changes with the dc gain of the feedback controller, the following discussions will diverge into two classes according to the dc gain of the feedback controller.

2) Tracking Error Under the Feedback Controller With a Finite DC Gain:

When the dc gain of the feedback controller is finite, if feedforward control is not used, substituting (7) and (8) into (3), we can obtain

$$\begin{aligned} e(s) &\approx \frac{G_p^{-1}(s)}{G_c(0)} r(s) \approx \frac{(m_1 + m_2)}{G_c(0)} \left[s^2 + \frac{1}{\omega_n^2} s^4 - \frac{2\zeta_n}{\omega_n^3} s^5 \right] r \\ &= \frac{(m_1 + m_2)}{G_c(0)} \left[r^{(2)}(s) + \frac{1}{\omega_n^2} r^{(4)}(s) - \frac{2\zeta_n}{\omega_n^3} r^{(5)}(s) \right]. \end{aligned} \quad (10)$$

Equation (10) shows that the tracking error consists of terms proportional to derivatives of the reference trajectory. It can be proved that the magnitude of a lower order error term overwhelms that of higher order term (see Section II-E). Then, the tracking error can be approximated by

$$e(s) \approx \frac{(m_1 + m_2)}{G_c(0)} r^{(2)}(s). \quad (11)$$

Equation (11) shows that the tracking error is approximately proportional to the acceleration of the reference trajectory, which can be also validated with the simulation using the lead controller (corresponding to the finite dc gain), as shown in Fig. 5(a). The second-order tracking error term in (11) can be compensated by second-order feedforward, namely, acceleration feedforward as

$$F(s) = m_a s^2. \quad (12)$$

Substituting (7), (8), and (12) into (3), by a similar approximation, we can obtain

$$e(s) \approx \frac{[(m_1 + m_2) - m_a]}{G_c(0)} r^{(2)}(s). \quad (13)$$

Equation (13) shows that the tracking error is still approximately proportional to the acceleration with inaccurate acceleration feedforward, which can be easily validated by the simulation, as shown in Fig. 5(b). Once acceleration feedforward is well tuned, namely, $m_a \approx (m_1 + m_2)$, the effect of the second-order term in (10) is negligible, and the residual tracking error is dominated by the fourth-order term as

$$e(s) \approx \frac{(m_1 + m_2)}{G_c(0)} \frac{1}{\omega_n^2} r^{(4)}(s). \quad (14)$$

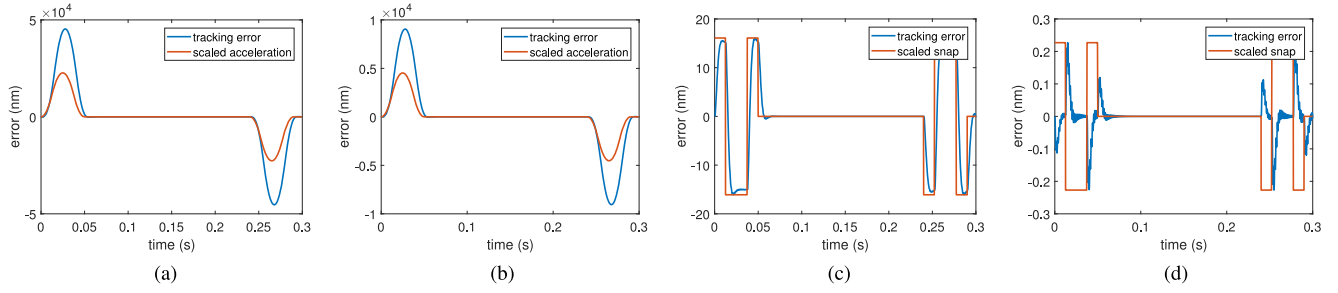


Fig. 5. Tracking error under the lead controller (corresponding to a finite dc gain). (a) No feedforward. (b) Inaccurate acceleration feedforward with $m_a = 20$ kg. (c) Accurate acceleration feedforward. (d) Accurate acceleration and snap feedforward.

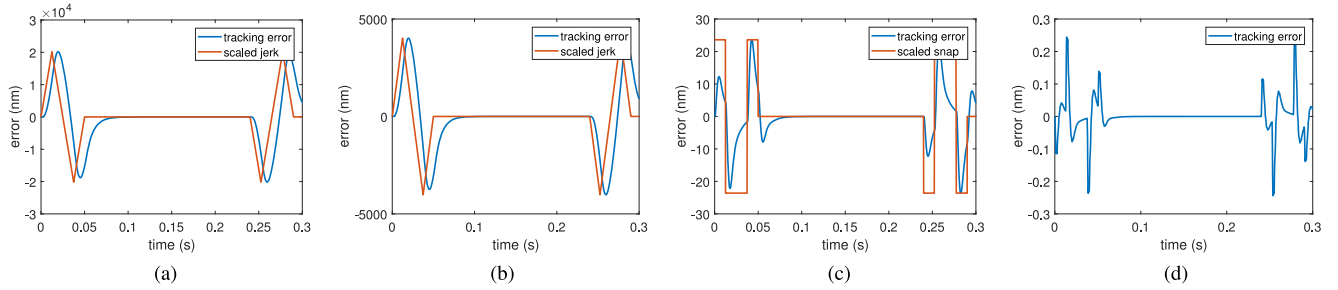


Fig. 6. Tracking error under the PID controller (corresponding to an infinite dc gain). (a) No feedforward. (b) Inaccurate acceleration feedforward with $m_a = 20$ kg. (c) Accurate acceleration feedforward. (d) Accurate acceleration and snap feedforward.

Equation (14) shows that the tracking error is approximately proportional to the snap of trajectory. The simulation result is given in Fig. 5(c). The fourth-order error term can be compensated by snap feedforward; then, the feedforward controller becomes

$$F(s) = m_a s^2 + m_s s^4. \quad (15)$$

Apparently, the accurate snap feedforward coefficient is the coefficient of the fourth-order term in the model inversion series (10)

$$m_s = \frac{(m_1 + m_2)}{\omega_n^2}. \quad (16)$$

Similarly, once snap feedforward is well tuned, the residual tracking error is dominated by the fifth-order term (the fifth derivative of the fourth-order trajectory can be regarded as a combination of impulses). The simulation result is given in Fig. 5(d).

Compensation of the residual tracking error after the use of acceleration and snap feedforward requires higher order feedforward. Note that snap feedforward requires the fourth derivable trajectory, and the trajectory order used in industry is usually equal to or lower than four in consideration of efficiency, disabling the utilization of high-order feedforward.

3) Tracking Error Under the Feedback Controller With an Infinite DC Gain: Disturbance rejection is indispensable for a practical control system, and the steady-state error is sometimes undesirable. Therefore, the feedback controller in practice often includes integral part, which makes the dc gain of the feedback controller infinite. The revised approximation of the input disturbance sensitivity function in (9) should be used in the analysis

of the tracking error instead of (8). By a similar deduction, it is not difficult to obtain that the tracking error with an inaccurate acceleration feedforward now becomes

$$e(s) \approx \frac{[(m_1 + m_2) - m_a]}{\tilde{G}_c(0)} r^{(3)}(s). \quad (17)$$

It means that the tracking error is approximately proportional to the jerk of trajectory; the simulation result is given in Fig. 6(a) and (b). With a well-tuned acceleration feedforward, the residual tracking error now becomes

$$e(s) \approx \frac{(m_1 + m_2)}{\tilde{G}_c(0)} \frac{1}{\omega_n^2} r^{(5)}(s). \quad (18)$$

It means that the residual tracking error is approximately proportional to the crackle of trajectory, which can be compensated by snap feedforward. The simulation result is given in Fig. 6(c).

D. Effect of ZOH and Time Delay on the Tracking Error

Most of the control systems, in practice, are digital control systems, which means ZOH exists between the controller and the plant model (see Fig. 7). Aside from this, time delay is inevitable for a practical control system due to mechanical and electrical factors. For ultraprecision motion systems with a nanoscale motion accuracy, even time delay of several sampling periods (several hundred microseconds) will lead to a big difference in the tracking error. The following analysis will show that the effect of ZOH and time delay will significantly influence the tracking error after tuning of acceleration feedforward and necessitate the use of jerk feedforward.

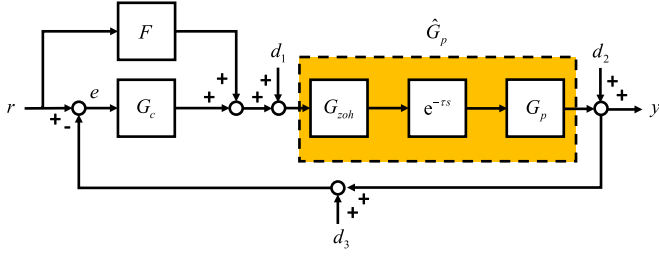


Fig. 7. Control architecture with the effect of ZOH and time delay.

For a digital control system with time delay, the equivalent plant model is

$$\hat{G}_p(s) = e^{-\tau s} G_{zoh}(s) G_p(s). \quad (19)$$

T is the sampling period, τ is the time delay, and $G_{zoh}(s)$ is the transfer function of ZOH

$$G_{zoh}(s) = \frac{1 - e^{-Ts}}{Ts}. \quad (20)$$

Then, the model inversion becomes

$$\begin{aligned} \hat{G}_p^{-1}(s) &= (m_1 + m_2)s^2 + \frac{1}{2}(T + 2\tau)(m_1 + m_2)s^3 \\ &+ \frac{(m_1 + m_2)(12 + T^2\omega_n^2 + 6T\tau\omega_n^2 + 6\tau^2\omega_n^2)s^4}{12\omega_n^2} \\ &+ o(s^5). \end{aligned} \quad (21)$$

Neglecting error terms higher than fourth order, the tracking error in (10) becomes

$$\begin{aligned} e(s) &\approx \frac{(m_1 + m_2)}{G_c(0)} \left[s^2 + \frac{(T + 2\tau)}{2}s^3 \right. \\ &\quad \left. + \frac{(12 + T^2\omega_n^2 + 6T\tau\omega_n^2 + 6\tau^2\omega_n^2)}{12\omega_n^2}s^4 \right] r \\ &= \frac{(m_1 + m_2)}{G_c(0)} \left[r^{(2)}(s) + \frac{(T + 2\tau)}{2}r^{(3)}(s) \right. \\ &\quad \left. + \frac{(12 + T^2\omega_n^2 + 6T\tau\omega_n^2 + 6\tau^2\omega_n^2)}{12\omega_n^2}r^{(4)}(s) \right]. \end{aligned} \quad (22)$$

It can be proved that the magnitude of the third-order error term in (22) is much smaller than that of the second-order term but can overwhelm fourth and higher order terms. Therefore, if the dc gain of the feedback controller is finite, the approximation of the residual tracking error with an accurate acceleration feedforward becomes

$$e(s) \approx \frac{(T + 2\tau)}{2} \frac{(m_1 + m_2)}{G_c(0)} r^{(3)}(s). \quad (23)$$

It shows that the residual tracking error is approximately proportional to the jerk of trajectory rather than snap when the effect of ZOH and time delay is considered [see Fig. 8(a)]. If the dc gain of the feedback controller is infinite and only one integrator exists, the approximation of the residual tracking error becomes

$$e(s) \approx \frac{(T + 2\tau)}{2} \frac{(m_1 + m_2)}{\tilde{G}_c(0)} r^{(4)}(s). \quad (24)$$

It shows that the residual tracking error is approximately proportional to the snap of trajectory rather than crackle when the effect of ZOH and time delay is considered [see Fig. 8(b)]. The effect of ZOH and time delay necessitates jerk feedforward; the feedforward controller structure then becomes

$$F(s) = m_a s^2 + m_j s^3 + m_s s^4. \quad (25)$$

Obviously, the accurate jerk feedforward coefficient is

$$m_j = \frac{(T + 2\tau)}{2} (m_1 + m_2). \quad (26)$$

After tuning of jerk feedforward, the error term that can be compensated by snap feedforward now becomes dominant in the residual tracking error shown in Fig. 8(c) and (d). An accurate snap feedforward coefficient is

$$m_s = \frac{(m_1 + m_2)(12 + T^2\omega_n^2 + 6T\tau\omega_n^2 + 6\tau^2\omega_n^2)}{12\omega_n^2}. \quad (27)$$

The terms related to T in feedforward coefficients can be regarded as the effect of ZOH, the terms related to τ can be regarded as the effect of time delay, and the terms related to ζ_n and ω_n can be regarded as the effect of plant dynamics.

E. Magnitudes of Different Error Terms

According to previous analysis, the tracking error can be decomposed into terms related to derivatives of trajectory. Furthermore, lower order terms overwhelm higher order terms in magnitude. For example, assuming that the dc gain of the feed-back controller is finite, the ratio of tracking error terms corresponding to jerk feedforward and acceleration feedforward can be easily attained from (22)

$$\frac{e_j(s)}{e_a(s)} = \frac{(T + 2\tau)}{2} \frac{r^{(3)}(s)}{r^{(2)}(s)}. \quad (28)$$

Convert back into time domain as

$$\frac{e_j(t)}{e_a(t)} = \frac{(T + 2\tau)}{2} \frac{r^{(3)}(t)}{r^{(2)}(t)}. \quad (29)$$

Assume $\tau = 2T$ and $T = 200 \mu s$, and choose a specific time instant, for example, the time jerk reaches its maximum when $\text{acc} = 5 \text{ m/s}^2$ and $\text{jerk} = 800 \text{ m/s}^3$. The ratio of $e_j(t)$ to $e_a(t)$ at the moment is 0.08, which is much smaller than 1. Similarly, it can be proved that the tracking error corresponding to snap feedforward is much smaller than $e_j(t)$.

F. General Deductions

Previous analysis is based on the noncollocated form of the double-mass-block model; the results will be generalized to the multimass-block model here. The key part of tracking error analysis is the approximation of the input disturbance sensitivity function S_i and plant model inversion. When it comes to the general multimass-block model, it is not hard to see that (8) and (9) can be still used as an approximation of S_i . As for plant model inversion, a fine approximation can be still attained at a low-frequency region by a Taylor series expansion at $s = 0$, though calculation will be a little more complicated. As shown in (2), the multimass-block model consists of a rigid body part

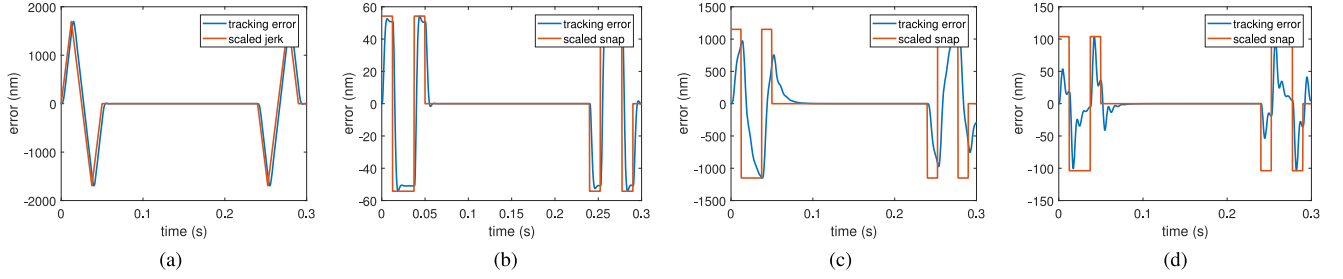


Fig. 8. Tracking error with the effect of ZOH and time delay considered, sampling period $T = 200 \mu\text{s}$, and time delay $\tau = 2T$. (a) Lead controller with accurate acceleration feedforward. (b) Lead controller with accurate acceleration and jerk feedforward. (c) PID controller with accurate acceleration feedforward. (d) PID controller with accurate acceleration and jerk feedforward.

and a resonant mode part as

$$G_p(s) = \frac{1}{ms^2} + \frac{1}{m} \sum_{i=1}^{N-1} \frac{\alpha_i}{s^2 + 2\zeta_i\omega_i s + \omega_i^2} = G_r(s) + G_f(s) \quad (30)$$

where

$$G_r(s) = \frac{1}{ms^2} \quad G_f(s) = \frac{1}{m} \sum_{i=1}^{N-1} \frac{\alpha_i}{s^2 + 2\zeta_i\omega_i s + \omega_i^2}. \quad (31)$$

The plant inversion of the multimass-block model can be then expressed as

$$\begin{aligned} G_p(s)^{-1} &= (G_r(s) + G_f(s))^{-1} \\ &= G_r(s)^{-1} \left(1 + G_r(s)^{-1} G_f(s) \right)^{-1} \\ &= ms^2 \left(1 + \sum_{i=1}^{N-1} \frac{\alpha_i s^2}{s^2 + 2\zeta_i\omega_i s + \omega_i^2} \right)^{-1} \\ &= ms^2 \left(1 + s^2 \tilde{G}_f(s) \right)^{-1} \end{aligned} \quad (32)$$

where $\tilde{G}_f(s) = mG_f(s)$. Equation (32) can be approximated by a series as follows:

$$ms^2 \left(1 + s^2 \tilde{G}_f \right)^{-1} = ms^2 \left(1 - s^2 \tilde{G}_f + s^4 \tilde{G}_f^2 - \dots \right). \quad (33)$$

$\tilde{G}_f(s)$ can be further expanded as

$$\begin{aligned} \tilde{G}_f(s) &= \sum_{i=1}^{N-1} \frac{\alpha_i}{s^2 + 2\zeta_i\omega_i s + \omega_i^2} \\ &= \sum_{i=1}^{N-1} \left\{ \frac{\alpha_i}{\omega_i^2} \left[1 - \left(\frac{2\zeta_i s}{\omega_i} + \frac{s^2}{\omega_i^2} \right) \right. \right. \\ &\quad \left. \left. + \left(\frac{2\zeta_i s}{\omega_i} + \frac{s^2}{\omega_i^2} \right)^2 + \dots \right] \right\}. \end{aligned} \quad (34)$$

Substituting (34) into (33), we can obtain

$$\begin{aligned} G_p(s)^{-1} &= ms^2 (1 + a_1 s^2 + a_2 s^3 + a_3 s^4 + \dots) \\ &= m (s^2 + a_1 s^4 + a_2 s^5 + a_3 s^6 + \dots). \end{aligned} \quad (35)$$

a_i is the model parameter determined by plant dynamics. Observing (34) and (33), it can be found that the existence of damping leads to the occurrence of odd-order terms in plant inversion (35). The transfer function of ZOH and time delay can also be expanded as

$$\begin{aligned} (G_{\text{zoh}}(s) e^{-\tau s})^{-1} &= \left(\frac{1 - e^{-Ts}}{Ts} e^{-\tau s} \right)^{-1} \\ &= 1 + \left(\frac{T}{2} + \tau \right) s + \frac{(T^2 + 6T\tau + 6\tau^2)}{12} s^2 \\ &\quad + \frac{1}{12} (T^2\tau + 3T\tau^2 + 2\tau^3) s^3 + \dots \end{aligned} \quad (36)$$

Combining (35) and (36), we can obtain the plant inversion with ZOH and time delay considered

$$\begin{aligned} (\hat{G}_p(s))^{-1} &= (e^{-\tau s} G_{\text{zoh}}(s) G_p(s))^{-1} \\ &= m \left(s^2 + \left(\frac{T}{2} + \tau \right) s^3 + \hat{a}_1 s^4 + \hat{a}_2 s^5 + \dots \right). \end{aligned} \quad (37)$$

\hat{a}_i is the model parameter determined by plant dynamics, ZOH, and time delay. Note that it is the effect of ZOH and time delay that leads to the occurrence of the third-order term in the equivalent plant model inversion. With the approximation of S_i and plant model inversion, assume that no feedforward is used; substituting (8) and (37) into (3), we can obtain an approximation of the tracking error under the feedback controller with a finite dc gain

$$e(s) \approx \frac{m}{G_c(0)} \left(r^{(2)}(s) + \frac{T+2\tau}{2} r^{(3)}(s) + \hat{a}_1 r^{(4)}(s) + \dots \right). \quad (38)$$

Equation (38) shows that the tracking error consists of different error terms related to the derivatives of the reference trajectory. Subsequent deductions on the tracking error under different feedforward controllers and a feedback controller with an infinite dc gain are almost the same with those on the tracking error

TABLE II
SHAPE OF THE TRACKING ERROR UNDER DIFFERENT CONDITIONS

Feedforward Controller	Feedback Controller	
	finite DC gain	infinite DC gain
inaccurate acceleration feedforward	acceleration	jerk
accurate acceleration feedforward	jerk	snap
accurate acceleration and jerk feedforward	snap	crackle
accurate acceleration, jerk and snap feedforward	crackle	pop

of the noncolocated double-mass-block model and thus will be omitted here. Explicit expressions of model parameters like \hat{a}_i in (37) can be attained once the transfer function of the plant model is given. However, such a calculation is, to some extent, unnecessary for feedforward tuning, and this will be discussed in detail in Section III.

G. Generation Mechanism

In conclusion, the generation mechanism of the tracking error during the acceleration or deceleration phase in ultraprecision motion systems can be stated as follows.

- 1) The tracking error during the acceleration or deceleration phase can be decomposed into terms related to derivatives of the reference trajectory, and lower order error terms overwhelm higher order terms in magnitude. The dc gain of the feedback controller, the order of the feedforward controller, and the accuracy of feedforward coefficients greatly influence the shape of the tracking error in the time domain. With given feedback and feedforward controllers, the tracking error is approximately proportional to a specific-order derivative of trajectory. In other words, the shape of the tracking error is similar to that of a specific derivative of trajectory in the time domain with given feedforward and feedback controllers (see Table II).
- 2) The effect of ZOH and time delay in a digital control system also greatly influences the tracking error, necessitating jerk feedforward rather than snap feedforward once acceleration feedforward is well tuned. And, snap feedforward will also be influenced by ZOH and time delay, not just by resonant dynamics.
- 3) According to the constructions of feedforward coefficients, acceleration feedforward compensates for rigid body dynamics, jerk feedforward for the effect of ZOH and time delay, and snap feedforward for part of resonant dynamics and the effect of ZOH and time delay.

III. FEEDFORWARD TUNING ALGORITHM

The quantitative analysis in Section II can not only interpret the generation mechanism of the tracking error, but can also give rise to a feedforward tuning algorithm by dichotomy.

The analysis in Section II provides a criterion to judge the accuracy of feedforward coefficients that can be used for feedforward tuning. For example, if the dc gain of the feedback controller is finite, first, initialize acceleration feedforward with

Algorithm 1: Feedforward Tuning Algorithm by Dichotomy.

```

1: Initialize acceleration feedforward by system identification
   or other methods
2: while the shape of tracking error is similar to acceleration
   (jerk) of trajectory do
3:   Change acceleration feedforward coefficient by di-
   chotomy
4: end while
5: if tracking error is small enough then
6:   Tuning finished
7: else
8:   while the shape of tracking error is similar to jerk
   (snap) of trajectory do
9:     Change jerk feedforward coefficient by dichotomy
10:   end while
11: end if
12: if tracking error is small enough then
13:   Tuning finished
14: else
15:   while the shape of tracking error is similar to snap
   (crackle) of trajectory do
16:     Change snap feedforward coefficient by dichotomy
17:   end while
18: end if
19: Tuning finished

```

Fig. 9. Feedforward tuning algorithm under the feedback controller with a finite dc gain. The content in parenthesis corresponds to the feedback controller with an infinite dc gain.

system identification or by equation

$$\tilde{m}_a = \frac{e(t) G_c(0)}{r^{(2)}(t)} \quad (39)$$

which can be derived from (11) or (13). The initial acceleration feedforward may well suffer from inaccuracy. Use dichotomy to tune acceleration feedforward as long as the tracking error has the shape of acceleration of the reference trajectory, once the shape of the residual tracking error becomes similar to the jerk of the reference trajectory; it means that acceleration feedforward is well tuned. Next, tune jerk feedforward; according to (23) and (26), jerk feedforward can be initialized by

$$\tilde{m}_j = \frac{e(t) G_c(0)}{r^{(3)}(t)}. \quad (40)$$

Use dichotomy to tune jerk feedforward until the shape of the residual tracking error becomes similar to the snap of reference trajectory; a similar approach applies for snap feedforward tuning. The complete algorithm is given in Fig. 9. Derivatives of the reference trajectory can be directly used as input signals for the feedforward controller if the trajectory is planned in advance. Otherwise, a real-time difference on the reference trajectory should be executed to attain such signals.

This algorithm has been proved quite effective in several engineering practices. Note that the trajectory varies in different applications, for situation where the acceleration and higher order derivatives of the trajectory are relatively small; a well-tuned acceleration feedforward is enough to provide good tracking

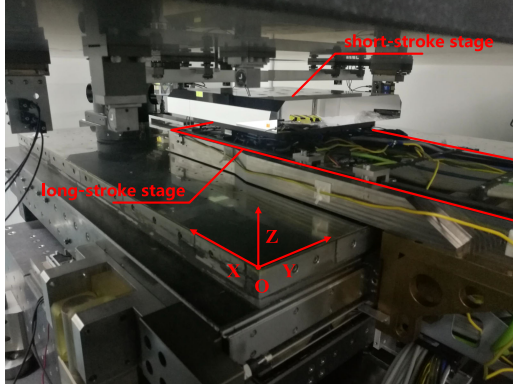


Fig. 10. Experimental platform. The ultraprecision motion system is actuated by six-DOF magnetic-levitated planar motors.

performance during the acceleration or deceleration phase, for situation where large acceleration and higher order derivatives are required, and tuning of jerk and snap feedforward may be needed.

IV. EXPERIMENT

A. Experiment Platform

The tracking control experiment is carried on the ultraprecision motion system shown in Fig. 10. The system consists of a long-stroke stage and a short-stroke stage, both stages are actuated by six-DOF magnetic-levitated planar motors. The long-stroke stage is used to realize long-stroke motion of micrometer-scale accuracy, while the short-stroke one is used to realize short-stroke motion of nanoscale accuracy. The displacement of the mirror block on the short-stroke stage is measured by a laser interferometer with a resolution of 0.15 nm. The mirror block and the motor mover of the short-stroke stage theoretically constitute a double-mass-block model. The sampling period of the control system is 200 μ s (5 kHz). The experiment is carried on axis x .

B. System Identification and Feedback Controller Design

Fig. 11 shows the system identification result of axis x ; the -40 -dB/dec slope at a low-frequency range corresponds to the rigid body mode. The primary resonant mode occurs at around 670 Hz, and other resonant modes exist. The phase lag that can be clearly observed in the bode diagram at a low-frequency region shows the very existence of time delay.

Instead of the lead controller and the PID controller used in theoretical analysis, a double-lead controller is used as a feedback controller with a finite dc gain

$$G_c(s) = K \left(\frac{s + z_1}{s + p_1} \right)^2. \quad (41)$$

A PI plus double-lead controller (a PI controller combined with a double-lead controller) is used as a feedback controller with an infinite dc gain

$$G_c(s) = K \frac{s + z_0}{s} \left(\frac{s + z_1}{s + p_1} \right)^2. \quad (42)$$

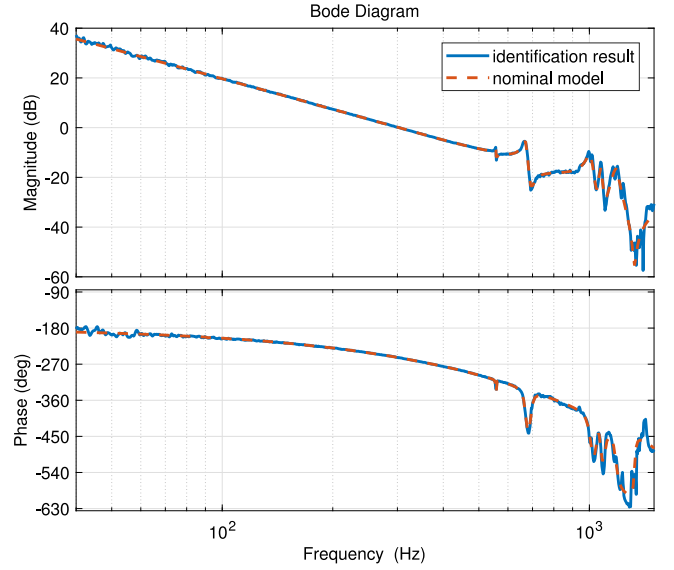


Fig. 11. System identification of axis x .

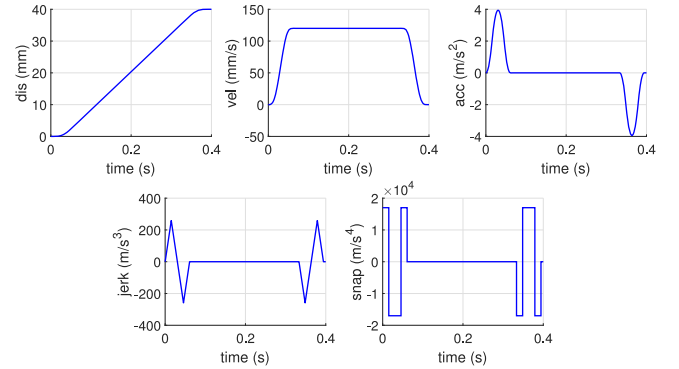


Fig. 12. Reference trajectory used in the experiment, dis bound 40 mm, vel bound 120 mm/s, acc bound 4 m/s², jerk bound 260 m/s³, and snap bound 17 000 m/s⁴.

The control bandwidth of both controllers is 240 Hz. The controllers are designed according to the nominal model from system identification. Though controllers used in the experiment are different from those used in the simulation, it is the dc gain not the specific form of the feedback controller that matters. Therefore, the results in previous sections still stand.

C. Experimental Results

The trajectory used in the experiment is shown in Fig. 12. Experimental results are given in Figs. 13 and 14. As theoretical analysis predicted, if no feedforward is used, the tracking error is approximately proportional to the acceleration of the reference trajectory under the feedback controller with a finite dc gain [see Fig. 13(a)] to jerk of reference trajectory under the feedback controller with an infinite dc gain [see Fig. 14(a)]. Figs. 13(b) and 14(b) give the tracking performance with acceleration feedforward attained from system identification. The explicit decrease of the tracking error during the acceleration or deceleration phase shows that the tracking error has been effectively attenuated by acceleration feedforward. However,

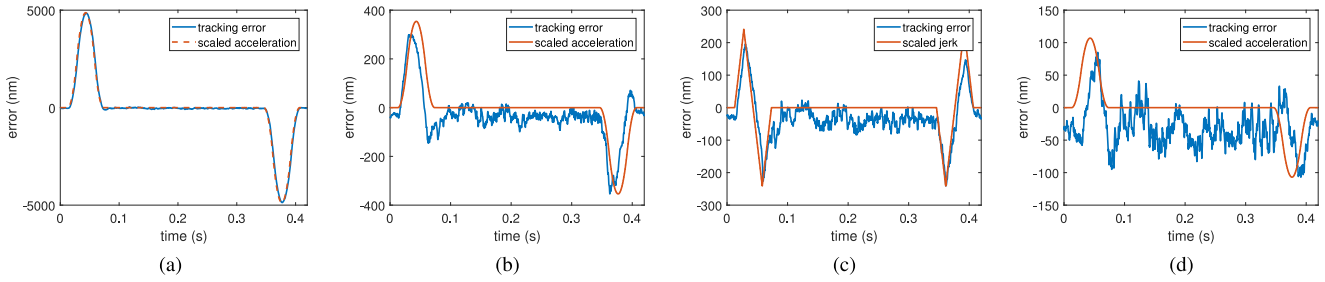


Fig. 13. Tracking error under the double-lead controller (corresponding to a finite dc gain). (a) No feedforward. (b) Acceleration feedforward (feedforward coefficient is from system identification). (c) Accurate acceleration feedforward tuned by dichotomy. (d) Accurate acceleration and jerk feedforward.

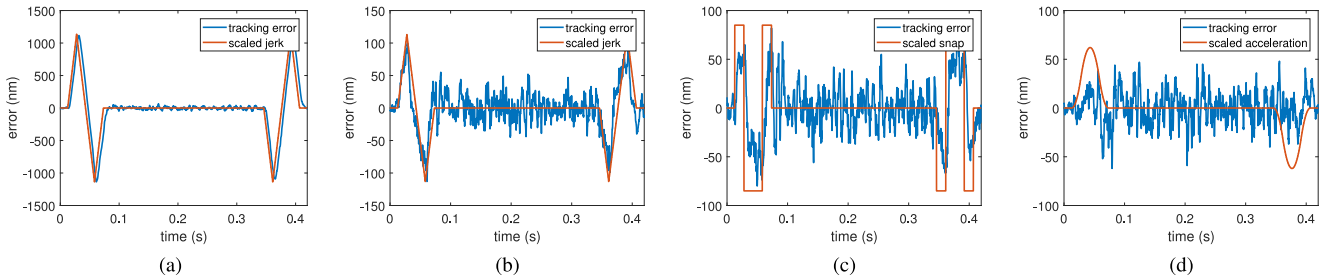


Fig. 14. Tracking error under PI + double-lead controller (corresponding to an infinite dc gain). (a) No feedforward. (b) Acceleration feedforward (feedforward coefficient is from system identification). (c) Accurate acceleration feedforward tuned by dichotomy. (d) Accurate acceleration and jerk feedforward.

the shape of the residual error manifests the inaccuracy of the acceleration feedforward coefficient. Acceleration feedforward can be easily tuned by dichotomy. Change acceleration feedforward until the residual tracking error has the shape of higher order derivatives of trajectory. Once the shape of the residual tracking error is similar to the jerk of trajectory under the feedback controller with a finite dc gain [see Fig. 13(c)], to snap of trajectory under the feedback controller with an infinite dc gain [see Fig. 14(c)], it means that acceleration feedforward is well tuned and further performance enhancement requires jerk feedforward. Jerk feedforward can be tuned in the same way, and Figs. 13(d) and 14(d) give the tracking performance with well-tuned acceleration and jerk feedforward. Due to external disturbance, the steady-state error exists if the feedback controller contains no integral part [see Fig. 13(d)]. It can be seen that the tracking error and the settling time have been greatly reduced. Since the tracking performance during the acceleration phase parallels that of the constant velocity phase, there is no need for use of snap feedforward.

V. FURTHER DISCUSSIONS

A. Scope of Applications and Limitations

Though the simulation and the experiment both well validate the theoretical analysis, some further discussions on the scope of applications and limitations about the generation mechanism and proposed algorithm need to be made.

- 1) The analysis and algorithm apply for friction-free motion systems, where the rigid body mode exists. This condition can be satisfied in ultraprecision motion systems like the motion stage of a lithography machine and hard-disk

drives. For systems with linear damping from the environment, -20 -dB/dec dynamics will replace -40 -dB/dec rigid body mode at a low-frequency region. By the same methodology, it can be proved that a new error term related to the velocity of the reference trajectory if the dc gain of the feedback controller is finite, to acceleration if the dc gain of the feedback controller is infinite, will occur and can be compensated by velocity feedforward. However, in practice, friction from the environment is usually much more complicated than linear damping. In this situation, the methodology may not work as well as it did in friction-free systems.

- 2) The plant model in the simulation and the motion system in the experiment are both lightly damped, but the generation mechanism also applies for systems with a large structural damping, for example, $\zeta_n = 0.7$. It can be proved that the structural damping will appear in terms higher than fourth order in plant model inversion, and the corresponding error terms are much smaller than lower order terms in magnitude even when the damping is large. Therefore, the generation mechanism still stands for a large structural damping.
- 3) Notch filters are widely used in the feedback controller design for systems with flexibility. The generation mechanism and the proposed algorithm still stand under the feedback controller with notch filters, since the notch filter does not affect the dc gain of the feedback controller. Moreover, notch filters are usually utilized at around resonant frequencies of the plant model, higher than the low-frequency region where most of the energy of the reference trajectory distributes. Such a property can

further guarantee the validity of the proposed methodology under the feedback controller with notch filters.

- 4) Well-tuned acceleration, jerk, and snap feedforward are able to provide a good approximation of plant inversion at a low-frequency region. In situations where the reference trajectory has very large derivatives and thus contains nonnegligible high-frequency components, more advanced control algorithms may be required for further compensation, since higher order feedforward is usually infeasible in practice due to limited derivability of the reference trajectory in consideration of efficiency.

B. Comparison With Other Feedforward Strategies

Aside from the proposed feedforward algorithm in this paper, there are several other effective model-based feedforward strategies: stable-inversion feedforward like zero-phase-error tracking control (ZPETC) and zero-magnitude-error tracking control (see [14] and [15]); and model-based feedforward with input shaping (see [4] and [6]). The primary distinctions between these approaches can be stated as follows.

- 1) For ultraprecision motion control, one of the most indispensable parts of all these approaches is tuning. Manual tuning of methods like ZPETC or feedforward with input shaping is a kind of difficulty that data-based techniques are usually utilized for tuning (see [4], [6], and [16]). From this perspective, the algorithm proposed in this paper enjoys a better understanding of physics and thus convenience of implementation and tuning.
- 2) Time delay is treated from different perspectives. ZPETC handles delay by noncausal feedforward, input shaping handles delay by shifting reference trajectory, and the proposed algorithm handles delay by jerk feedforward and adjustment of snap feedforward.
- 3) The capability of approximating plant inversion differs. As discussed in Section V-A, unless higher order derivable trajectory is utilized to enable higher order feedforward at expense of efficiency, the capability of approximating plant inversion at a high-frequency region is limited for the proposed algorithm. With an appropriate feedforward controller structure, ZPETC and feedforward with input shaping have the potential to approximate plant inversion at a high-frequency region, though data-based methods, more often than not, have to be utilized to exploit this potential. This difference matters if the reference trajectory has very large derivatives and thus contains nonnegligible components at a high-frequency region.

On the whole, all these approaches have respective advantages, which one to use can be determined by specific applications.

VI. CONCLUSION

This paper mainly focused on the generation mechanism of the tracking error during the acceleration or deceleration phase in a kind of ultraprecision motion systems those are actuated by levitated linear or planar motors and thus render friction from

the environment negligible. The analytical relationship among the tracking error, the feedforward controller, the feedback controller, and the reference trajectory was presented for the first time. Analysis shows that the tracking error is approximately proportional to a specific derivative of the reference trajectory with given feedback and feedforward controllers. In other words, the tracking error has a similar shape of a specific derivative of the trajectory, and the derivative order is decided by feedforward and feedback controllers used. Due to the effect of ZOH and time delay, it is jerk rather than snap feedforward proposed in previous research studies that is responsible for the attenuation of the dominant part in the residual tracking error once acceleration feedforward is well tuned. The shape of the residual tracking error can be used as a criterion to judge the accuracy of feedforward coefficients. Based on this criterion, a feedforward tuning algorithm using dichotomy was proposed. The simulation and experiment both well validate the analysis on the generation mechanism of the tracking error and the proposed feedforward tuning algorithm. The proposed tuning algorithm is a manual tuning one due to its reliance on the subjective criterion such as the similarity of shape. Automation of the tuning procedure will be studied in the future research.

REFERENCES

- [1] H. Butler, "Position control in lithographic equipment [applications of control]," *IEEE Control Syst.*, vol. 31, no. 5, pp. 28–47, Oct. 2011, doi: [10.1109/mcs.2011.941882](https://doi.org/10.1109/mcs.2011.941882).
- [2] M. Boerlage, R. Tousain, and M. Steinbuch, "Jerk derivative feedforward control for motion systems," in *Proc. Amer. Control Conf.*, 2004, vol. 5, pp. 4843–4848.
- [3] M. Boerlage, M. Steinbuch, and G. Angelis, "Frequency response based multivariable control design for motion systems," in *Proc. IEEE Conf. Control Appl.*, 2005, pp. 980–985, doi: [10.1109/cca.2005.1507257](https://doi.org/10.1109/cca.2005.1507257).
- [4] M. Heertjes and D. Bruijnen, "MIMO FIR feedforward design for zero error tracking control," in *Proc. Amer. Control Conf.*, Jun. 2014, pp. 2166–2171, doi: [10.1109/acc.2014.6858752](https://doi.org/10.1109/acc.2014.6858752).
- [5] M. Heertjes, D. Hennekens, and M. Steinbuch, "MIMO feed-forward design in wafer scanners using a gradient approximation-based algorithm," *Control Eng. Practice*, vol. 18, no. 5, pp. 495–506, May 2010, doi: [10.1016/j.conengprac.2010.01.006](https://doi.org/10.1016/j.conengprac.2010.01.006).
- [6] F. Boeren, D. Bruijnen, N. van Dijk, and T. Oomen, "Joint input shaping and feedforward for point-to-point motion: Automated tuning for an industrial nanopositioning system," *Mechatronics*, vol. 24, no. 6, pp. 572–581, Sep. 2014, doi: [10.1016/j.mechatronics.2014.03.005](https://doi.org/10.1016/j.mechatronics.2014.03.005).
- [7] Y. Jiang, K. Yang, Y. Zhu, X. Li, and D. Yu, "Optimal feedforward control with a parametric structure applied to a wafer stage," *Proc. Inst. Mech. Eng. I, J. Syst. Control Eng.*, vol. 228, no. 2, pp. 97–106, Nov. 2013, doi: [10.1177/0959651813506897](https://doi.org/10.1177/0959651813506897).
- [8] H. Butler, "Adaptive feedforward for a wafer stage in a lithographic tool," *IEEE Trans. Control Syst. Technol.*, vol. 21, no. 3, pp. 875–881, May 2013, doi: [10.1109/tcst.2012.2188102](https://doi.org/10.1109/tcst.2012.2188102).
- [9] D. Yu, Y. Zhu, K. Yang, C. Hu, and M. Li, "A time-varying q-filter design for iterative learning control with application to an ultraprecision dual-stage actuated wafer stage," *Proc. Inst. Mech. Eng. I, J. Syst. Control Eng.*, vol. 228, no. 9, pp. 658–667, Aug. 2014, doi: [10.1177/0959651814547443](https://doi.org/10.1177/0959651814547443).
- [10] D. Bristow, M. Tharayil, and A. Alleyne, "A survey of iterative learning control," *IEEE Control Syst. Mag.*, vol. 26, no. 3, pp. 96–114, Jun. 2006, doi: [10.1109/mcs.2006.1636313](https://doi.org/10.1109/mcs.2006.1636313).
- [11] D. K. Miu, *Mechatronics: Electromechanics and Contrmechanics*. New York, NY, USA: Springer, 2012.
- [12] A. Preumont, *Vibration Control of Active Structures*. Dordrecht, The Netherlands: Springer, 2011.
- [13] P. Lambrechts, M. Boerlage, and M. Steinbuch, "Trajectory planning and feedforward design for electromechanical motion systems," *Control Eng. Practice*, vol. 13, no. 2, pp. 145–157, Feb. 2005, doi: [10.1016/j.conengprac.2004.02.010](https://doi.org/10.1016/j.conengprac.2004.02.010).

- [14] B. Rigney, L. Pao, and D. Lawrence, "Nonminimum phase dynamic inversion for settle time applications," *IEEE Trans. Control Syst. Technol.*, vol. 17, no. 5, pp. 989–1005, Sep. 2009, doi: [10.1109/tcst.2008.2002035](https://doi.org/10.1109/tcst.2008.2002035).
- [15] M. Tomizuka, "Zero phase error tracking algorithm for digital control," *J. Dyn. Syst., Meas., Control*, vol. 109, no. 1, pp. 65–68, 1987, doi: [10.1115/1.3143822](https://doi.org/10.1115/1.3143822).
- [16] M. Li, Y. Zhu, K. Yang, C. Hu, and H. Mu, "An integrated model-data-based zero-phase error tracking feedforward control strategy with application to an ultraprecision wafer stage," *IEEE Trans. Ind. Electron.*, vol. 64, no. 5, pp. 4139–4149, May 2017, doi: [10.1109/tie.2016.2562606](https://doi.org/10.1109/tie.2016.2562606).
- [17] Y. Jiang, Y. Zhu, K. Yang, C. Hu, and D. Yu, "A data-driven iterative decoupling feedforward control strategy with application to an ultraprecision motion stage," *IEEE Trans. Ind. Electron.*, vol. 62, no. 1, pp. 620–627, Jan. 2015.
- [18] Z.-S. Hou and Z. Wang, "From model-based control to data-driven control: Survey, classification and perspective," *Inf. Sci.*, vol. 235, pp. 3–35, 2013.
- [19] F. Boeren, L. Blanken, D. Bruijnen, and T. Oomen, "Optimal estimation of rational feedforward control via instrumental variables: With application to a wafer stage," *Asian J. Control*, vol. 20, pp. 975–992, May 2018.
- [20] M. Iwasaki, K. Seki, and Y. Maeda, "High-precision motion control techniques: A promising approach to improving motion performance," *IEEE Ind. Electron. Mag.*, vol. 6, no. 1, pp. 32–40, Mar. 2012.
- [21] X. Li, K. Yang, Y. Zhu, and D. Yu, "Feedforward coefficient identification and nonlinear composite feedback control with applications to 3-DOF planar motor," *J. Mech. Sci. Technol.*, vol. 27, no. 3, pp. 895–907, Mar. 2013.
- [22] X. Li, K. Yang, Y. Zhu, and D. Yu, "Non-linear composite control with applications to 3-DOF planar motor," *Trans. Inst. Meas. Control*, vol. 35, no. 3, pp. 330–341, May 2012.
- [23] L. Dai, X. Li, Y. Zhu, and M. Zhang, "A high performance feedforward tuning approach for ultra-precision motion control," in *Proc. 32nd ASPE Annu. Meeting*, 2017, pp. 439–444.
- [24] D. Torfs, J. Swevers, and J. D. Schutter, "Quasi-perfect tracking control of non-minimal phase systems," in *Proc. 30th IEEE Conf. Decis. Control*, 1991, pp. 241–244.
- [25] L. Blanken, F. Boeren, D. Bruijnen, and T. Oomen, "Batch-to-batch rational feedforward control: From iterative learning to identification approaches, with application to a wafer stage," *IEEE/ASME Trans. Mechatronics*, vol. 22, no. 2, pp. 826–837, Apr. 2017.
- [26] C. Hu, Z. Wang, Y. Zhu, M. Zhang, and H. Liu, "Performance-oriented precision LARC tracking motion control of a magnetically levitated planar motor with comparative experiments," *IEEE Trans. Ind. Electron.*, vol. 63, no. 9, pp. 5763–5773, Sep. 2016.
- [27] J. Anthonis and H. Ramon, "Linear mechanical systems and dyadic transfer function matrices," *Automatica*, vol. 39, no. 8, pp. 1353–1363, Aug. 2003.
- [28] Z. Hou, H. Gao, and F. L. Lewis, "Data-driven control and learning systems," *IEEE Trans. Ind. Electron.*, vol. 64, no. 5, pp. 4070–4075, May 2017.
- [29] S. Yin, X. Li, H. Gao, and O. Kaynak, "Data-based techniques focused on modern industry: An overview," *IEEE Trans. Ind. Electron.*, vol. 62, no. 1, pp. 657–667, Jan. 2015.
- [30] M. Boerlage, "MIMO jerk derivative feedforward for motion systems," in *Proc. Amer. Control Conf.*, 2006, p. 6.
- [31] G. M. Clayton, S. Tien, K. K. Leang, Q. Zou, and S. Devasia, "A review of feedforward control approaches in nanopositioning for high-speed SPM," *J. Dyn. Syst., Meas., Control*, vol. 131, no. 6, 2009, Art. no. 061101.
- [32] C.-H. Menq and J. Jae Chen, "Precision tracking control of discrete time nonminimum-phase systems," *J. Dyn. Syst., Meas., Control*, vol. 115, no. 2A, pp. 238–248, 1993.



Luyao Dai received the B.S. degree in mechanical engineering in 2016 from Tsinghua University, Beijing, China, where he is pursuing the Ph.D. degree in mechanical engineering from the Department of Mechanical Engineering.

His research interests include ultraprecision motion control.



Xin Li received the B.S. and M.S. degrees in mechanical engineering from the Dalian University of Technology, Dalian, China, in 2006 and 2009, respectively, and the Ph.D. degree in mechanical engineering from Tsinghua University, Beijing, China, in 2013.

He is currently an Assistant Professor with the Department of Mechanical Engineering, Tsinghua University. He has authored or coauthored more than ten papers and applied for more than ten invention patents. His research interests include precision/ultraprecision motion control and robot control, especially the control and application of precision motion systems for engineering practice in industry.



Yu Zhu (M'12) received the B.S. degree in radio electronics from Beijing Normal University, Beijing, China, in 1983, and the M.S. degree in computer applications and the Ph.D. degree in mechanical design and theory from the China University of Mining and Technology, Beijing, in 1993 and 2001, respectively.

He is currently a Professor with the State Key Laboratory of Tribology, Department of Mechanical Engineering, Tsinghua University, Beijing.

He has authored more than 180 technical papers. He holds more than 50 warranted invention patents. His research interests include precision measurement and motion control, ultraprecision mechanical design and manufacturing, two-photon microfabrication, and electronics manufacturing technology and equipment.



Ming Zhang received the B.S. degree in mechanical engineering from the University of Science and Technology Beijing, Beijing, China, in 1996, and the Ph.D. degree in precision instruments from Tsinghua University, Beijing, in 2005.

He is currently an Associate Professor with the Department of Mechanical Engineering, Tsinghua University. His research interests include ultraprecision mechanical design and manufacturing, system modeling and analysis, and design of high-precision linear motors and planar motors.



Chuxiong Hu (S'09–M'11–SM'16) received the B.S. and Ph.D. degrees in mechatronic control engineering from Zhejiang University, Hangzhou, China, in 2005 and 2010, respectively.

From 2007 to 2008, he was a Visiting Scholar in mechanical engineering with Purdue University, West Lafayette, IN, USA. He is currently an Associate Professor with the Department of Mechanical Engineering, Tsinghua University, Beijing, China. His research interests include

precision/ultraprecision motion control, high-performance multiaxis contouring control, precision mechatronic systems, robots, adaptive robust control, iterative learning control, deep learning, neural networks, nonlinear systems, and precision metrology/measurement calibration.

Prof. Hu is the recipient of the Best Student Paper Finalist at the 2011 American Control Conference, the 2012 Best Mechatronics Paper Award from the ASME Dynamic Systems and Control Division, the 2013 National 100 Excellent Doctoral Dissertations Nomination Award of China, and the 2016 Best Automation Paper Award from the IEEE International Conference on Information and Automation.